Materials Science in Semiconductor Processing 190 (2025) 109312

Contents lists available at ScienceDirect

Materials Science in Semiconductor Processing

journal homepage: www.elsevier.com/locate/mssp

Proton irradiation effects on silicon heterojunction solar cells with MoO_x selective contacts

S. Duarte-Cano [a], F. Pérez-Zenteno [a], D. Caudevilla [a], J. Olea [a], E. San Andrés [a], A. del Prado [a], R. Benítez-Fernández [a], E. García-Hemme [a], M. Rezaei [b], J.A. Clemente [b], S. Algaidy [c], I. Torres [d], R. Barrio [d], E. Ros [e], J. Puigdollers [e], P. Ortega [e], C. Voz [e], R. García-Hernansanz [a,*]

[a] Dpto. EMFTEL, Fac. CC. Físicas, Univ. Complutense de Madrid, Madrid, Spain
[b] Dpto. ACYA, Fac. Informática, Univ. Complutense de Madrid, Madrid, Spain
[c] Instituto de Energía Solar, Universidad Politécnica de Madrid, E.T.S.I. Telecomunicación, 28040, Madrid, Spain
[d] Dpto. de Energías Renovables, CIEMAT, Madrid, Spain
[e] Dpt. d'Enginyeria Electrònica. Universitat Politècnica de Catalunya, Barcelona, Spain

ARTICLE INFO

Keywords:
Photovoltaic
Defect
Proton irradiation
Recombination centers
Solar cell
Transition metal oxides

ABSTRACT

In this study, we investigate the effects of proton irradiation on silicon-based heterojunction and molybdenum oxide (MoO_x) selective contact solar cells. The main idea is to study their potential application in small satellites for measurement and monitoring. The irradiation dose simulates the aggressive environment found in Low Earth Orbit (LEO), where many satellites currently use Group III-VI (GaInP/GaAs/Ge) solar cells due to their superior efficiency, albeit at a higher cost. The experimental approach includes fabrication, irradiation, and characterization methods. Our results show a decrease in fill factor (F.F.) and overall efficiency after irradiation, mainly caused by a decrease in shunt resistance and an increase in series resistance. In addition, open-circuit voltage (V_{oc}) and short-circuit current (I_{sc}) may be affected by displacement damage defects caused by the irradiation process within the active region or by the formation of new point defects.

1. Introduction

Since the launch of the Vanguard-1 satellite in 1958, which pioneered the integration of monocrystalline Si solar cells into its power system [1–4] there has been a concerted drive to investigate innovative photovoltaic (PV) configurations tailored to space applications. This search for improved designs is intended to boost the efficiency and reliability of PV systems in the challenging environment of outer space. The relentless pursuit of advances in solar cell technology is motivated by the need to continuously optimize the performance and durability of solar power generation in space, thereby ensuring maximum functionality of satellites and other spacecrafts.

Recent advances in photovoltaic technology have focused on enhancing the durability and efficiency of solar cells under extreme conditions [5–7]. However, the long-term impact of proton irradiation remains underexplored. One prominent approach in this field involves utilizing a combination of GaInP, GaAs, and Ge materials, resulting in a highly efficient solar cell of 32 % under Air mass 0 (AM0) (1 sun, 136 mW/cm^2) conditions [8–12]. However, the drawback associated with this approach is the high cost of these technologies. Therefore, researchers have been exploring alternative options based on silicon cells, which, although typically less resistant to radiation [13–15], can offer comparable efficiency at a reduced budget [16].

Silicon-based solar cells present a compelling alternative due to their relative affordability and widespread availability. TMO (transition metal oxides) heterojunction silicon solar cells have attracted considerable scientific attention. These cells exhibit several advantages over traditional silicon homojunction solar cells. One key advantage is the manufacturing process, as TMO materials can be synthesized at lower temperatures ranging from 100 to 200 °C [17,18]. This contrasts with the higher temperatures typically required for manufacturing diffusion homojunction silicon solar cells.

Transition metal oxides, such as MoO_x, have been extensively researched for their potential applications in various fields. Studies have shown that MoO_x can serve as hole-selective contact, leading to improvements in device performance and stability in applications like

* Corresponding author.
E-mail address: rodgar01@ucm.es (R. García-Hernansanz).

https://doi.org/10.1016/j.mssp.2025.109312
Received 7 October 2024; Received in revised form 10 December 2024; Accepted 16 January 2025

organic solar cells, organic light-emitting diodes, and thin film transistors [19–21]. Furthermore, TMO heterojunction silicon solar has shown good reliability, which can be explained by the stability of these inorganic selective contacts [22,23]. Also, MoO_x has recently been shown to improve the stability and protection of perovskite solar cells/absorbers, that indicates an important potential in space applications [24–26].

This study hypothesizes that silicon-based solar cells with MoO_x selective contacts will exhibit greater resilience to proton irradiation. The primary objectives are to quantify the degradation in efficiency and to identify structural changes post-irradiation. To achieve this goal, we studied the results of a controlled proton-induced damage process on a Heterojunction with Intrinsic Thin layer (HIT) silicon solar cell compared to the case of implementing a MoO_x selective contact. The proton irradiation energy used in this study aimed to simulate radiation conditions like those present in Low Earth Orbit (LEO) [27].

The design of HIT solar cells has been modified structurally, incorporating MoO_x-based selective contacts to achieve cost reductions. This is accomplished by utilizing fewer critical materials by operating at lower temperatures, which results in energy savings compared to traditional diffusion cells. Additionally, these modifications aim to enhance radiation resistance for greater stability without substantially compromising the solar cell efficiency. The use of MoO_x as a selective contact material has shown potential for improving carrier collection [20,23,28,29] and reducing recombination losses, essential for achieving higher conversion efficiencies in solar cells. Un-irradiated cells were previously studied in the references mentioned before [20,23,29,30].

The main purpose of this work is to test the degradation of MoO_x and HIT solar cells when they are subjected to similar conditions to space radiation. Our research on the effect of proton irradiation on solar cells involved the study of their Current Density-Voltage (J-V) characteristics before and after irradiation. This analysis focuses on the understanding of the performance of the cells under simulated AM0 illumination conditions. We gained insight into the influence of the solar cell reverse saturation current and overall diode characteristics through a detailed examination of the J-V behavior in both illumination and darkness conditions. This methodology allowed us a comprehensive evaluation of the effects of proton irradiation on the functionality and quality of the solar cells.

These findings are important for the development of cost-effective radiation-tolerant solar cells, particularly in the context of space applications. Specifically, the challenges presented by irradiation conditions in LEO need thorough studies to guarantee the long-term performance and reliability of photovoltaic systems in space.

2. Experimental

We fabricated HIT solar cells using a p-type crystalline silicon substrate with a resistivity of 2.6 Ω cm and 300 μm thick. The substrate undergoes a sequence of treatments, including an RCA cleaning process and immersion in a 1 % hydrofluoric acid (HF) solution, until achieving a hydrophobic state. Subsequently, the treated substrate is introduced into a Plasma-Enhanced Chemical Vapor Deposition (PECVD) system, where multiple layers are deposited on the backside. The layered configuration comprised a 4-nm (4 nm) passivation layer of intrinsic amorphous silicon (a-SiC_x:H), serving the dual purpose of safeguarding the stack and acting as a coating for the back reflector (BRC). After this, the backside underwent laser-firing, inducing locally diffused point contacts. This process yielded a contact area ratio of 0.5 %. The laser procedure achieved a minimal series resistance while keeping low surface recombination in the back contact where is deposited Al. An n-type a-Si:H/intrinsic a-Si:H stack was deposited on the top surface to create the Heterojunction structure. The structure was finalized depositing the antireflective conductive indium tin oxide (ITO) layer by RF magnetron sputtering, and a thermal evaporation process was employed to define the finger bus of the top layer with Ag. The fabrication route of the HIT solar cells follows process reported in [31,32].

For MoO_x solar cells, the n-Si wafers (1.5 Ω cm, 280 μm thick) were textured by alkaline etching and cleaned using the RCA method and a 1 % HF immersion. The substrates were then immediately loaded into a PECVD system to deposit a layer stack on the back side. This stack included a 4 nm a-SiC_x (x∼0.2) intrinsic passivation layer, a 15 nm phosphor-doped a-Si layer and an 80 nm a-SiC_x (x∼1) backside reflector. The backside was subsequently subjected to a laser triggering process to create a locally diffuse point contact array. After a second immersion in 1 % HF, 15 nm of MoO_x was thermally evaporated over the front face (8×10^{-6} mbar, 0.2 Å/s). After a brief exposure to air, an anti-reflective ITO front electrode was deposited by RF magnetron sputtering. After lithographic patterning of 1 cm^2 active cell areas, metallization of the back contact was performed by electron beam evaporation of titanium (15 nm) and thermal evaporation of aluminum (1 μm), while the silver grating of the front contact was thermally evaporated. The fabrication route of the MoO_x solar cells follows the process reported in Refs. [33,34].Fig. 1 shows the structure of the HIT and MoO_x solar cells.

To replicate the effect of radiation in LEO orbit, these devices have been subjected to two proton irradiations at two laboratories. Firstly, the samples (HIT & MoO_x) were irradiated at the Cyclone Cyclotron Accelerator at Centro Nacional de Aceleradores (CNA) in Sevilla, Spain, with protons, reaching a total fluence of 1.26×10^{10} p/cm^2 at 15 MeV. The proton beam form 90° with solar cell surface and impacts through the front face (ITO) of the cell. When the results were subjected to joint analysis with the RD50 team at CERN [35] it was found that the equivalent displacement damage exceeded 4.25×10^{10} 1-MeV neutrons/cm^2 [36]. A second irradiation process was carried out at the Institute of Nuclear Physics of the Czech Academy of Sciences (CAS) in Prague using the U-120M cyclotron and an X-Y positioning device with a rectangular collimator. The samples were exposed to a significant dose of 2.1×10^9 p/cm^2 at 16 MeV in this phase. In both irradiation steps, the cells were completely covered by the beam. The values used in each radiation step are recorded in Table 1.

Furthermore, it is important to note that the samples were exposed to an approximate total ionizing dose of nearly 6 krad, which is equivalent to the radiation exposure experienced by an object in space over 8.5 years [37]. Such exposure is crucial for evaluating the long-term durability and performance of materials intended for space applications.

In both irradiation cases, meticulous attention was given to the experimental setup to ensure that maximum displacement damage was induced in the samples, adhering to industry standards and guidelines. To achieve this, the terminals of the samples were deliberately grounded during the irradiation process. Grounding the terminals dissipates any accumulated charge or electrical potential within the samples, thereby allowing a more accurate assessment of the displacement damage caused by the energetic particles [38].

Cell characterization was performed after each irradiation step. Measurements were made both in the absence of light and under

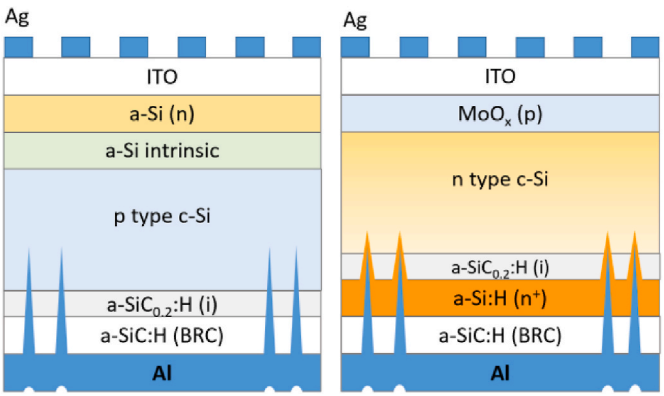

Fig. 1. Structures of HIT solar cell (left) and MoO_x solar cell (right).

Table 1
Irradiation steps.

Radiation step	Fluence (p/cm2)	Energy (MeV)	IEDD[a]	Ionizing dose (krad)
CNA	1.26×10^{10}	15	4.25×10^{10}	5.12
CAS	2.10×10^{9}	16	6.91×10^{9}	0.81
Total			4.94×10^{10}	5.93

[a] IEDD: Individual Equivalent Displacement damage (1-MeV neutrons/cm^2).

illumination. Characterization was performed only after the radioisotopes were deactivated (typically we measured 10 days after the irradiation processes). This procedure ensured that any transient defects were eliminated.

The J-V curves under illumination were measured at room temperature (25 °C) and with adjusted AM0 spectral conditions. The samples were placed in a Class A Steuernagel Lichttechnik SC-575 solar simulator. The front and back contact was made on the fingers through a 3-wire system. This setup allowed the variation of current and voltage parameters.

Dark J-V measurements were performed at various temperatures within a helium closed-cycle Janis cryostat using a Keithley 4200-SCS (Semiconductor Characterization System). The 2-diode solar cell-circuit equivalent model [39–41] was utilized to fit the results, with forward and reverse response currents adjusted throughout the temperature range (340-220 K).

Transmission electron microscopy (TEM) measurements were performed using a JEOL 2100 HT microscope, operated at 200 kV and using a double-tilt sample holder to orient the lamella. For XEDS analysis we used an Oxford Instruments INCA microanalysis system at ICTS – Centro Nacional de Microscopia Electrónica.

3. Results

Montecarlo simulations using SRIM (Stopping and Range of Ions in Matter) software were used to model the effects of proton impact. In Fig. 2, we present the proton trajectory on complete solar cell structure a), and the first 145 nm (active area) of the solar cell b). In Fig. 2 a) we can observe that almost all the total ions cross the solar cell. Indeed, the projected range of protons in a silicon substrate is 1440 **μm**. Therefore, we can conclude that the damage is distributed throughout the material.

In Fig. 3 we present the vacancies caused by proton collisions in the MoO_x cell. In Fig. 3 a) we can observe the damage caused in the active area of the cell and in 3 b) the full cell. We can observe that the damage caused in ITO and MoO_x layers is lower than Si substrate damage. Regarding the MoO_x layer, we can observe that the radiation caused vacancies concentration in the order of 10^4 cm^{-3} across whole layer. As the electrical behavior of this material depends highly of O vacancies, a change in it is expected. In Fig. 3 b), it is clear than the vacancies created across the whole cell is always lower than 10^6 cm^{-3} and almost constant. Similar results were obtained for HIT solar cell structure.

TEM images of both cells (before and after irradiation) are presented in Fig. 4 for MoO_x solar cell. Similar results were obtained for HIT cell. Image a) displays the microstructure before any irradiation process, while image b) shows the microstructure after the CAS step irradiation (Table 1). TEM procedures for measurements before irradiation and after the second irradiation step were conducted on different cells fabricated using identical processes.

Fig. 4 reveals no significant observable variations in the HIT cell after the irradiation steps. The analysis performed for the MoO_x sample in Fig. 4 shows a thin layer of silicon oxide (SiO_x) despite being subjected to HF [42,30,41] treatment before the deposition processes. The spontaneous regrowth of a thin silicon oxide interlayer upon MoO_x deposition has been explained in a previous work [43]. In addition, no

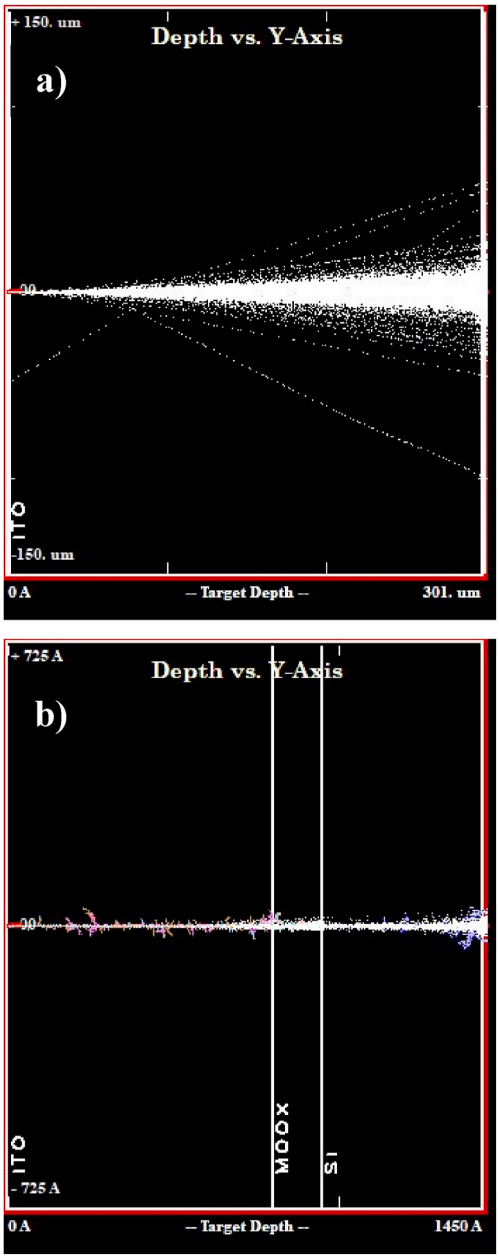

Fig. 2. a) Proton trajectory on MoO_X solar cell obtained by Montecarlo SRIM simulation. b) Proton trajectory on active area of the same cell.

significant variations in the 2 nm native oxide layer were observed in the irradiation processes undergone.

By comparing images (a) and (b), it is evident that no visible change or damage occurs in the crystal structure of c-Si, the amorphous layers, or the thin native oxide layers after the irradiation processes. No extended defects, such as stacking faults or dislocations, are observed after all the irradiation steps. The insets of Fig. 4 show the diffraction pattern of the c-Si region, confirming that the crystalline structure is maintained in this region of the solar cell. Point defects may not be large or coherent enough to affect diffraction patterns. Additionally, the defects generated may be uniformly and sparsely distributed within the material structure, rendering them undetectable by TEM.

Fig. 5a) and b) and Table 2, present the J-V characteristics under illumination of the HIT and the MoO_x cells, respectively. For each figure, we present the current density variation as a function of voltage after each step of irradiation received.

First, we observe that the open circuit voltage (V_{oc}) and short circuit

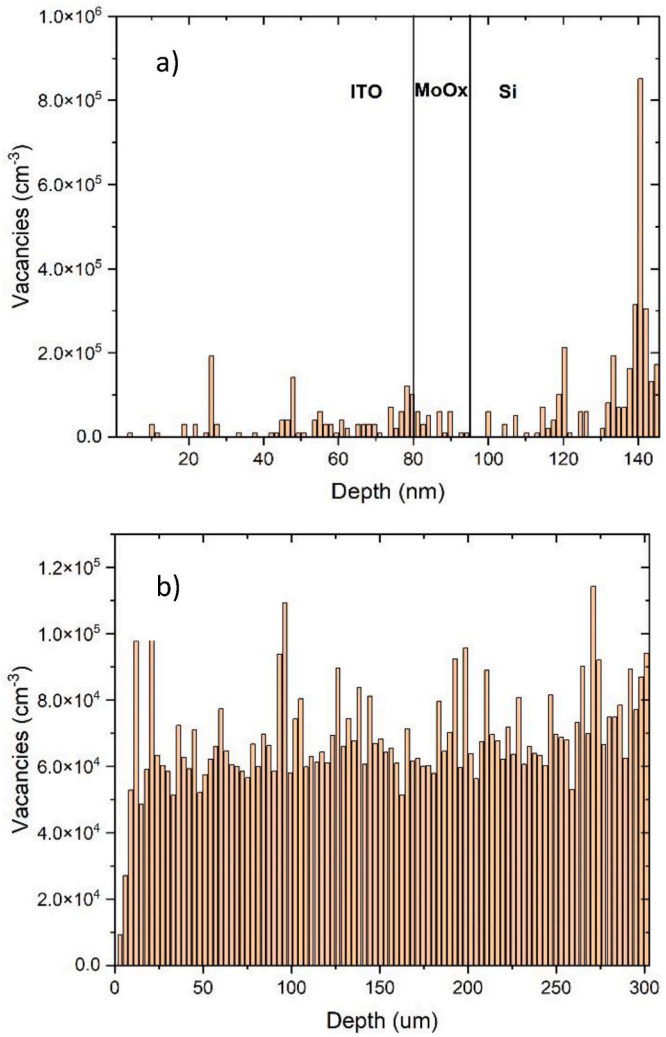

Fig. 3. Number of vacancies obtained by SRIM simulation for a) active region of the cell and, b) whole the cell.

current density (J_{sc}) do not show significant changes after the first irradiation step. However, the F.F. deteriorates significantly. Our observations revealed a significant increase in series resistance accompanied by a noteworthy decrease in shunt resistance. Both contribute to a substantial deterioration of the fill factor and therefore the overall efficiency of the cells is significantly degraded. Furthermore, by exposing the solar cells to additional proton irradiation at a higher cumulative dose of 5.93 krad, we observe a further degradation of the F.F., the V_{oc}, and, mainly in the I_{sc} values. Proton irradiation caused consistent degradation trends in both types of cells, resulting in an efficiency loss of almost 50 % of their initial value.

In Fig. 6 we present the EQE of MoO_x solar cell before and after been radiated. We can observe a decrease in the EQE for all wavelengths, that is an indication that the cell was damaged throughout its volume. This result is in full agreement with SRIM simulation, where we previously observed almost constant damage across the whole cell. However, if we obtained how much change the EQE after radiation at each wavelength (inset on Fig. 6) in percent, we obtain more deviation at high and low wavelengths. This result could indicate than radiation damages the passivation at the front and at back contacts of the cell specifically.

Fig. 7 a) and b) show dark J-V measurements for the HIT cell and the MoO_x cell respectively, at room temperature. For both cells, J-V characteristics are presented for each different irradiation step. Solid dark lines show the results of numerical fittings, which will be discussed in the next section. For these fittings the two diodes model was used.

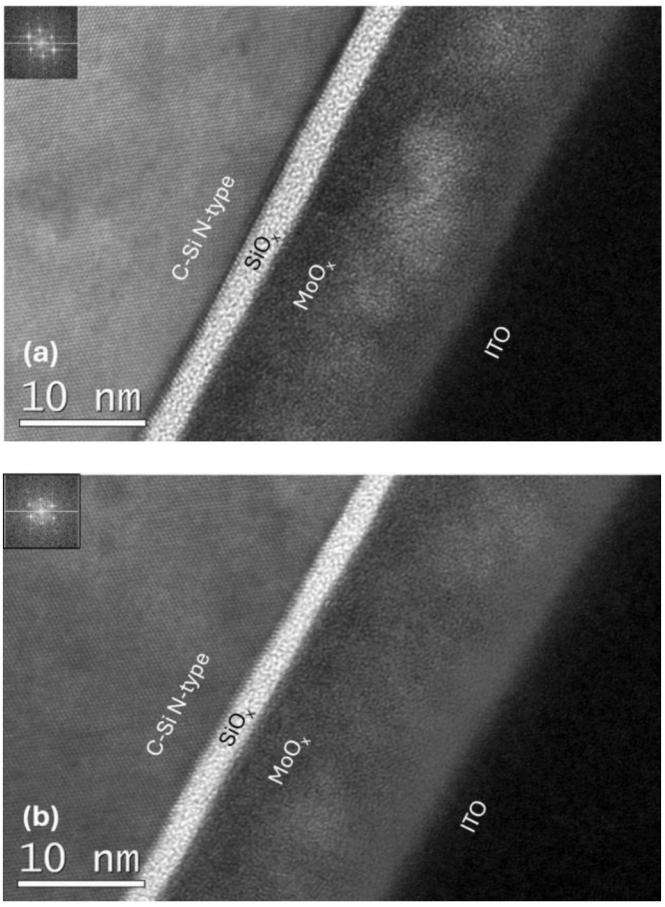

Fig. 4. TEM for MoO_x *solar cells. Reference condition (up) after CAS step irradiation (5.93* krad*) (down). Samples with a zoom on C-Si Type layer to Optical diffraction view.*

From these figures, it is evident that with each irradiation step, there are significant changes in the shape of the J-V curves at different bias regimes. In the high positive bias region (>0.6 V), we can observe a decrease in the current values as the irradiation dose increases, which indicates an increase in the series resistance. Regarding the low bias region (<0.6 V) we can observe an important increase in the current value for the last irradiation step. In the same way, at reverse bias we can observe an increase in the current values as the irradiation dose grows. The next section will discuss all these changes in the framework of changes in the dominant electronic transport mechanisms.

4. Discussion

First, we will refer to the results of the solar cell in illumination. The decrease of the short-circuit current in the HIT and MoO_x cells could be attributed to displacement damage in the active region of the devices caused by proton irradiation. This damage may create point defects, reducing the lifetime of the light-generated minority carriers, and thereby decreasing the collection efficiency of photogenerated carriers [40,44]. This scenario correlates well with the observed reduction of the V_{oc}, which is very sensitive to recombination processes. The reduction in lifetime due to the creation of point defects will lead to higher recombination, which will ultimately cause the V_{oc} reduction [45]. This result is in full agreement with the EQE decrease observed for the irradiated cell on Fig. 7. As we exposed before, the passivation of the cell at the front and back structure is possible.

We should consider different parameters to discuss the observed decrease in F.F. as the irradiation dose increases. First, radiation

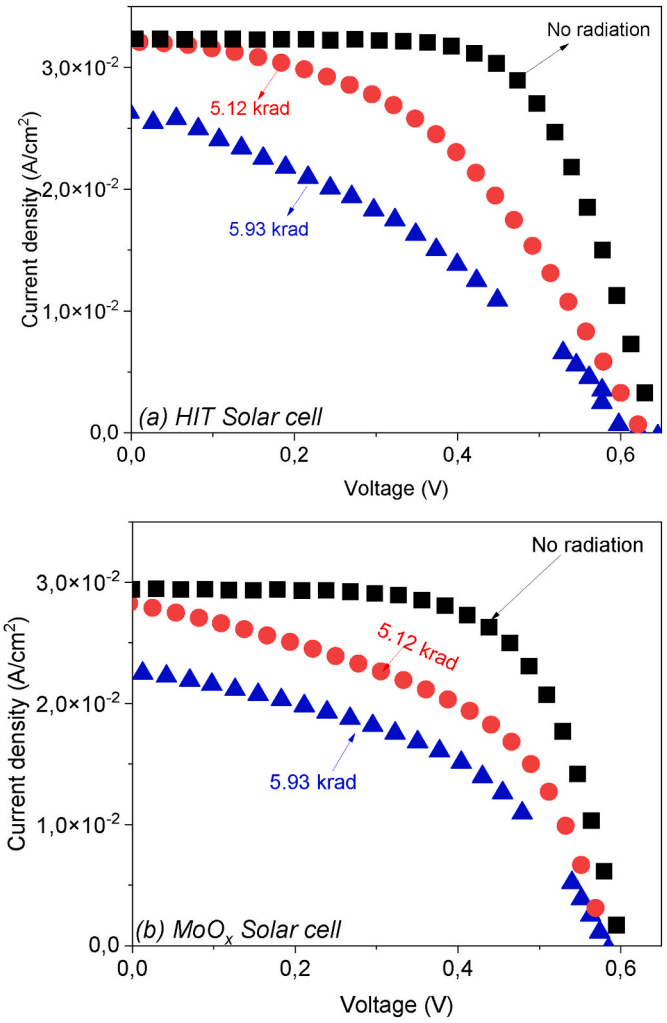

Fig. 5. HIT(a) and MoO_x (b) solar cell, J-V illumination curves before and after each irradiation step.

Table 2
Electrical parameters at different irradiation steps on HIT and MoO_x solar cells.

Sample	V_{oc} (V)	J_{sc} (A)	FF	η (%)	R_s (Ω)	R_{sh} (Ω)
HIT No irradiation	0.63	0.032	0.67	10.2	4.4	4798
HIT (5.12 krad)	0.62	0.032	0.46	6.8	8.4	176
HIT (5.93 krad)	0.61	0.025	0.36	4.2	15	106
MoO_x No irradiation	0.6	0.029	0.66	8.6	3.8	2130
MoO_x (5.12 krad)	0.57	0.028	0.51	5.9	6	64
MoO_x (5.93 krad)	0.56	0.022	0.47	4.5	8.4	80

exposure can induce various mechanisms that elevate R_s [46]. One potential factor is the degradation of ITO conductivity [47,48] which lead to a significant increases in R_s [40,49] Also, it is possible a radiation-induced degradation in the transport properties of the metal electrodes [50,51] Another important factor which can increase the series resistance is the radiation-induced deactivation of dopants within the silicon bulk, potentially phosphorus or boron [48]. The irradiation processes can lead to the deactivation of dopants in both crystalline silicon (c-Si) and amorphous silicon (a-Si). This deactivation results in a reduction of the built-in potential of the junction, which is influenced by the product of the acceptor (N_A) and donor (N_D) concentrations [52]. Studies have shown that the deactivation of dopants in silicon substrates can occur due to the preferential relocation of dopant atoms slightly displaced from lattice sites, forming clusters that contribute to electrical deactivation [53]. Furthermore, in Ref. [54], it is highlighted that the

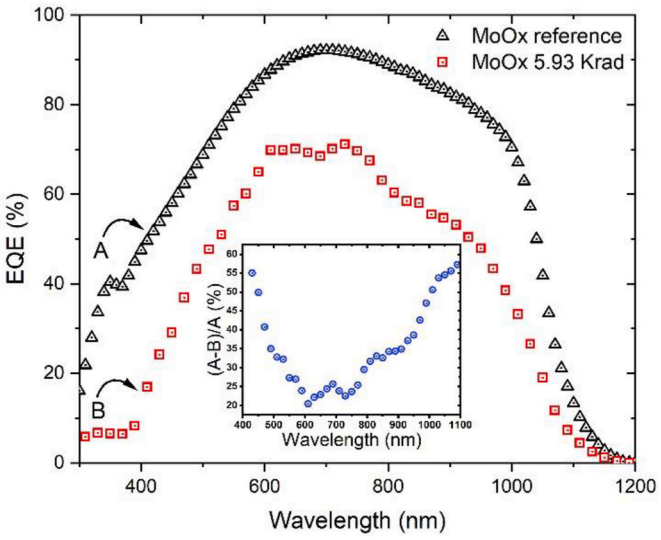

Fig. 6. EQE of MoOx solar cell before and after irradiation. In the inset we can observe the difference between the EQE before radiation and after radiation, in percentage. We can observe that this difference is high at low and high wavelengths.

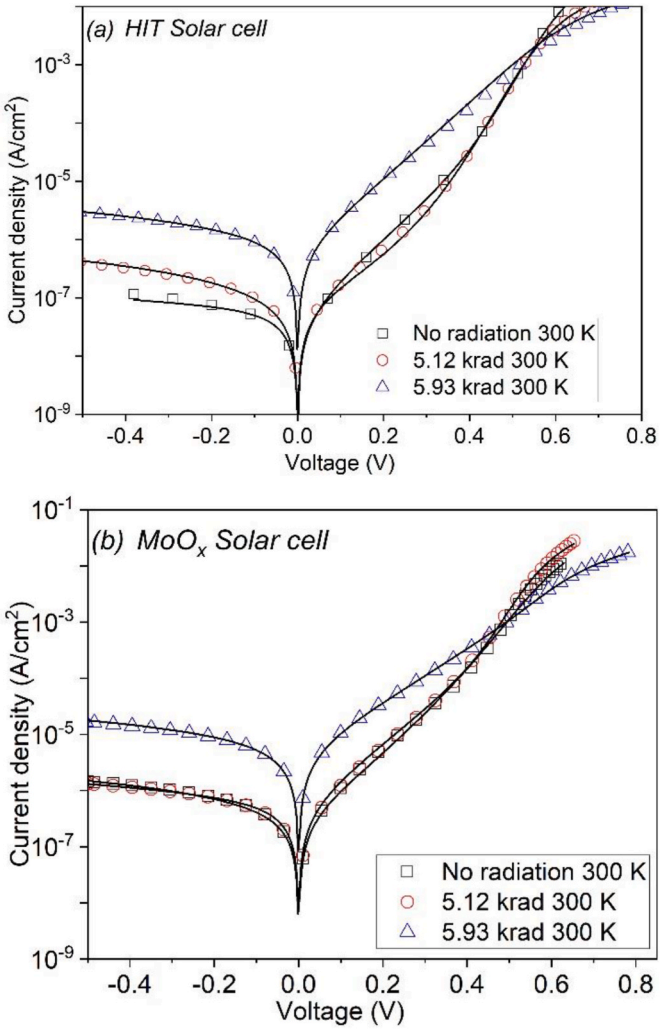

Fig. 7. Relationship between current density (J) and voltage (V) for an (a) HIT and (b) MoO_x solar cell under different irradiation conditions.

deactivation of dopants can occur due to the formation of dopant-defect complexes, leading to reduced electrical activation. Additionally, the presence of defects such as donor-pair-vacancy-interstitial complexes can contribute to dopant deactivation and impact the electrical activity of dopants [55]. Finally, the segregation of dopant atoms to interfaces, such as SiO_2/Si interfaces, can also lead to their deactivation [56,57].

Another factor which can lead to a F.F. reduction is a decrease in the solar cell shunt resistance. This shunt resistance decrease is usually directly related to the appearance of low-resistance alternative current paths through the junction or the cell borders. In our case, these new current paths could be related to the appearance and accumulation of point defects through the junction, either on the surface or at the interfaces between different layers. These point defects appear due to the irradiation process.

In addition to R_s and R_{shunt} degradation, changes in transport mechanisms could occur after radiation processes. To this end, we will discuss the dark J-V curves measured at various temperatures ranging from 220 K to 340 K. In most previous studies, two different current regimes have been observed in the forward bias direction for both HIT [58] and MoO_x solar cells [42,59]. To analyze these results, we used the accepted two diodes model for solar cells. To be consistent with the usual notation, the model is:

$$I = I_{diode1} + I_{diode2} + I_{shunt} \tag{1}$$

$$I = \boldsymbol{I}_{0,1}\left\{exp\left[\frac{q(V - IR_S)}{n_1 KT}\right] - 1\right\}$$

$$+\boldsymbol{I}_{0,2}\left\{exp\left[\frac{q(V - IR_S)}{n_2 KT}\right] - 1\right\} + \frac{V - IR_S}{R_P}$$

Here, I is the current across the cell, V the voltage at the cell electrodes, $I_{0,1}$ and $I_{0,2}$ denote the saturation currents and n_i is the ideality factor for each diode. At the same time R_s is the series resistance, R_{sh} denotes the parallel (shunt) resistance, k is Boltzmann's constant, and T is the absolute temperature in kelvin.

To fit the measurements, we used the numerical program *"2/3-Diode Fit"* [60], which is based on the work of Breitenstein and Riβland [61]. Lines in Fig. 6 are an example of the good agreement between fitting and measurements at room temperature. Similar fittings were obtained for all temperatures and radiation steps in this study and can be found in the supplementary material.

From these fittings, we obtained a diffusion process in the high bias region (V > 0,6 V) of the I-V, with a constant diode factor of $n_1 = 1$. We observed this process for both cells and for all radiation steps. The only effect we can observe that affects this diffusion process after radiation is the increase in series resistance. As diffusion process occurs on silicon bulk, we can conclude that the radiation does not affect it.

Regarding the low bias mechanisms (V < 0,6V) we cannot fit into a process with constant ideality factor n_2. Indeed, we obtain values much higher than 2, and with temperature dependence. Because of this, to analyze this transport process, it is better to fit to $A_2(T)$ (exponential factor in eq. (1)], which is the slope of the curves in logarithmic representation. $A_2(T)$ is defined as follows:

$$A_2(t) = \frac{q}{n_2 kT} \tag{2}$$

Fig. 8 shows the temperature dependence of this exponential factor $A_2(T)$ for this low forward bias region, for both cells and for all the radiation steps. To compare, we include in the graphs the value of $A_1(T)$ for the diffusion process (always the same for all radiation steps). In the HIT cell, we observe a rather constant value of $A_2(T)$ with temperature. This behavior is widely reported in different works as a tunnel process in silicon heterojunctions [62–66]. We can observe this behavior for all radiation steps, which may indicate that the transport mechanism which dominates conduction in this low bias regime does not change. However, although the slope does not change, the saturation current $I_{0,2}$ increases its value one order of magnitude after the last radiation step. In Fig. 7 this effect is clear. These two behaviors (same slope and more saturation current) combined, may indicate that the tunnel process remains after radiation, but it has been enhanced. Probably the radiation dose of 5.93 krad causes an increase in defects concentration at the heterojunction interface, in where tunnels in heterojunctions occur.

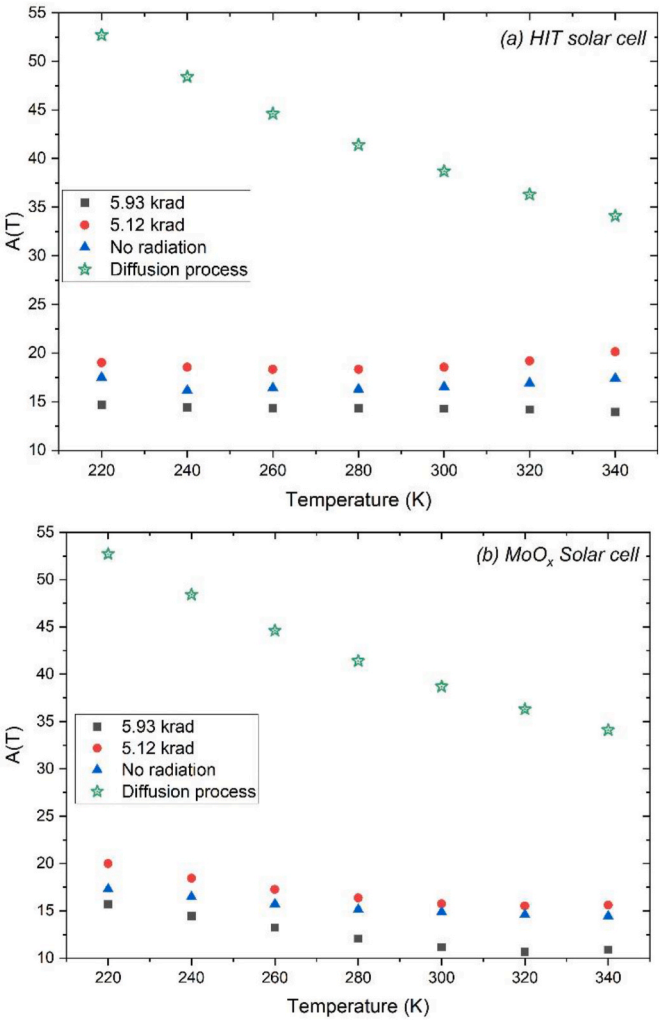

Fig. 8. Temperature dependence of the exponential factor $A_2(T)$ in the low forward bias region for an (a) HIT and (b)MoO_x, respectively, for cells after different irradiation conditions.

Same behavior can be observed in Fig. 8 (b) for the MoO_x based solar cell. In previous work [25], we determine multi-tunneling capture-emission (MTCE) as the most probably transport process in this region. Indeed, from SRIM simulation, we obtained that the defects concentration caused by irradiation was in the order of 10^5 cm^{-3}, that is not too high but probably high enough to explain this change in $I_{0,2}$.

For a better understanding of these transport processes, we have also analyzed the temperature dependence of the saturation current $I_{0,i}$. We present in the supplementary material, the fitted saturation current values (I_{01} and I_{02}) as a function of 1000/T, for both types of solar cells and for all radiation steps. From these fittings we obtained the activation energy $Ea_{,i}$ following Equation (3). The index i denotes the diffusion process (i = 1) or low bias process (i = 2).

$$I_{0,i} = I_{00,i}\, exp\left(-\frac{E_{a,I0i}}{kT}\right) \tag{3}$$

Fig. 9 presents the results for the activation energy of both transport mechanisms and both types of solar cells. As a first observation, the

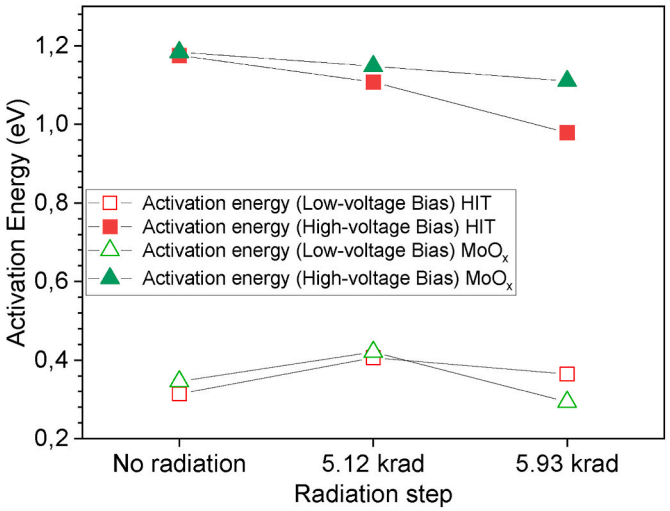

Fig. 9. Activation energy of the saturation current density for HIT and MoO_x solar cells.

irradiation process does not seem to produce significant changes in any of the activation energies, suggesting that the transport mechanisms for both diodes remain unmodified. Secondly, the activation energies obtained for low bias mechanism lies around 0.3–0.45 eV. These values are consistent with a tunnel process, and concretely with the MTCE tunnel proposed before. This process consists of multi-tunneling between gap states with subsequent recombination through carrier capture or reemission: a-Si:H gap states in the case of the HIT type solar cell [64,66,67] or the MoO_x gap states in MoO_x-type solar cells [21,22,30,68,69]. This is to be expected within the framework of the MTCE model, introduced by Matsuura et al. [70].

Finally, the activation energy of the high forward bias mechanism scatters around the c-Si band gap value of 1.12 eV. This result and the fixed ideality factor $n_1 = 1$ support the proposed model of the Shockley diffusion law governing the transport in the high-forward bias regime.

As we have previously discussed, the irradiation process does not seem to change the transport mechanisms identified. However, it could modify the prevalence of one mechanism over the other. We can observe that, independently of the type of solar cell, I_{01} slightly increases with the increase of the radiation dose, while I_{02} rises considerably it value after the second irradiation process. This indicates that the irradiation process produces a clear predominance of the tunnel mechanism over the diffusion process. This prevalence is so intense that for the case of the highest radiation dose, the tunneling mechanism masks the diffusion process in almost the whole J-V curve, as Fig. 7 shows.

The saturation current for the diffusion mechanism (I_{01}) is directly related to the diffusion length (Leff) in the neutral region of the crystalline silicon (c-Si) substrate. Therefore, the slight increase in I_{01} suggests that the irradiation process induces the formation of point defects in the c-Si bulk. These defects subsequently increase the density of recombination centers, thereby reducing the diffusion length within the substrate. Other works have shown that radiation can create defects such as vacancies and interstitials in the silicon lattice, which act as recombination centers [69]. These defects can trap carriers and facilitate non-radiative recombination, leading to an increase in the saturation current [71]. The density of these defects depends on the type of radiation and dose, which could correlate with the observed increase in I_{01}. [72].

The saturation current for the tunnel mechanism (I_{02}) is mainly related to the density of traps and gap states present in the MoO_x layer or in the a-Si layer (depends on solar cell type). The significant increase in I_{02} suggests that the irradiation process increases drastically the density of these gap states.

Radiation exposure has been shown to impact the atomic structure of various materials significantly. Furthermore, in the context of silicon, amorphous silicon has been observed to plastically deform under high-energy heavy ion irradiation, like conventional glasses [73] Moreover, the generation of point defects in crystalline silicon by heavy ions has been studied, highlighting the dose rate and temperature dependence of defect creation [74]. TMO's like MoO_x have shown dual behavior in terms of conductivity based on the doping levels. Studies have indicated that MoO_x can exhibit enhanced conductivity at low doses, attributed to improved hole collection and transport properties [75]. However, at higher doses, a degradation in conductivity might occur. This behavior is linked to the structure and composition of the material, where sub-stoichiometric molybdenum oxide has been identified as a high work function material that can efficiently enhance hole injection in various applications. This trend is commonly observed in transition metal oxides [76].

5. Conclusions

As a first conclusion, the results obtained indicate that silicon-based solar cell structures, either with MoO_x or HIT-type selective contacts, experience a degradation of approximately 50 % in their efficiency value when irradiated with a cumulative radiation dose equivalent to that received for 8.5 years when exposed to LEO conditions.

A detailed study of heterojunction solar cells under the influence of radiation has revealed several critical aspects concerning their performance deterioration and the predominant conduction mechanisms. The main aspects based on the points analyzed are as follows.

5.1. Impact on performance parameters

Initial degradation of cells under average radiation levels is mainly observed in the F.F. due to changes in R_s and R_{sh}. However, both I_{sc} and V_{oc} also show significant degradation under intense radiation conditions. This pattern suggests that intense and cumulative radiation causes more extensive and widespread damage to the cell.

5.2. Conduction mechanisms

Measurements in darkness and at various temperatures have confirmed the existence of two main conduction mechanisms in these heterojunction cells: Tunneling and diffusion at low and high forward bias, respectively. This finding corroborates previous knowledge on the behavior of heterojunction cells and contributes to understanding charge transport processes in these devices.

5.3. Effects of radiation on transport mechanisms

Despite exposure to different radiation levels, the basic transport mechanisms (tunneling and diffusion) do not appear to change. This result indicates that the fundamental nature of charge transport in heterojunction cells is robust to irradiation, which is a positive finding concerning material stability and cell design.

5.4. Change in the dominance of transport mechanisms

Although transport mechanisms remain unchanged, radiation affects the relative prevalence of these mechanisms. Radiation induces many traps/levels in the forbidden energy gap of MoO_x and amorphous silicon (a-Si). These defects facilitate multistep tunneling capture and emission (MTCE) process, thus modifying the charge transport dynamics and potentially influencing the overall efficiency.

CRediT authorship contribution statement

S. Duarte-Cano: Writing – review & editing, Writing – original draft, Visualization, Validation, Supervision, Software, Resources,

Investigation, Formal analysis, Data curation, Conceptualization. **F. Pérez-Zenteno:** Writing – review & editing, Investigation, Data curation. **D. Caudevilla:** Writing – review & editing, Investigation, Formal analysis, Data curation. **J. Olea:** Writing – review & editing, Resources, Methodology. **E. San Andrés:** Writing – review & editing, Project administration, Methodology, Funding acquisition, Conceptualization. **A. del Prado:** Writing – review & editing, Project administration, Funding acquisition, Conceptualization. **R. Benítez-Fernández:** Writing – review & editing, Investigation, Data curation. **E. García-Hemme:** Writing – review & editing, Project administration, Methodology, Formal analysis, Conceptualization. **M. Rezaei:** Writing – review & editing, Data curation, Conceptualization. **J.A. Clemente:** Writing – review & editing, Investigation, Data curation, Conceptualization. **S. Algaidy:** Writing – review & editing, Investigation. **I. Torres:** Writing – review & editing, Resources, Data curation. **R. Barrio:** Writing – review & editing, Resources, Investigation, Data curation. **E. Ros:** Writing – review & editing, Resources, Investigation, Data curation. **J. Puigdollers:** Writing – review & editing, Resources, Investigation, Funding acquisition. **P. Ortega:** Writing – review & editing, Resources, Investigation. **C. Voz:** Writing – review & editing, Resources, Investigation, Data curation, Conceptualization. **R. García-Hernansanz:** Writing – review & editing, Writing – original draft, Supervision, Investigation, Formal analysis.

Declaration of competing interest

The authors declare the following financial interests/personal relationships which may be considered as potential competing interests: Rodrigo Garcia-Hernansanz reports financial support was provided by Government of Spain. If there are other authors, they declare that they have no known competing financial interests or personal relationships that could have appeared to influence the work reported in this paper.

Acknowledgment

The authors would like to acknowledge the “CAI de Técnicas Físicas” of the Universidad Complutense de Madrid, ICTS – Centro Nacional de Microscopia Electrónica, to "Centro de Investigaciones Energéticas, Medioambientales y Tecnológicas" CIEMAT, Centro Nacional de Aceleradores (CNA), Institute of Nuclear Physics of the Czech Academy of Sciences (CAS) in Prague, and finally to RADNEXT TA04-43 for the support in resources and management of entities in the process of solar cell radiation with ASCUAS project. This activity has received funding from the European Union’s 2020 research and innovation program under grant agreement No 101008126, corresponding to the RADNEXT project.

This work was partially supported by the Spanish Research Agency (AEI, Ministry of Research and Innovation) and the European Regional Development Fund (ERDF) under grants PID2020-116508RB-I00, PID2020-117498RB-I00, PID2020-112916 GB-100 and PID2022-138434OB-C51.The authors also acknowledge financial support via research grants HyperSolar (TED2021-130894B-C21) and TransEL (TED2021-129758B-C32) funded by the Recovery and Resilience Facility of the EU.

F. Pérez-Zenteno is also thankful for financial collaboration from the Mexican grants program CONACyT and for a predoctoral contract from UCM (call CT58/21-CT59/21).

Sary Algaidy would also like to acknowledge financial support from the Ministry of Education in the Kingdom of Saudi Arabia.

R. Benítez-Fernández acknowledge the research contract under the Investigo Program (CT19/23-INVM-27) of the Ministerio de Trabajo y Economía Social.

Appendix A. Supplementary data

Supplementary data to this article can be found online at https://doi.org/10.1016/j.mssp.2025.109312.

Data availability

Data will be made available on request.

References

[1] V. Smil, The first PVS in orbit [Numbers Don’t Lie], IEEE Spectr 55 (3) (March 1958) 26, https://doi.org/10.1109/MSPEC.2018.8302382. Mar. 2018.
[2] N.D. Kaushika, A. Mishra, A.K. Rai, Repertoires of applications. Solar Photovoltaics, 2018, pp. 105–113, https://doi.org/10.1007/978-3-319-72404-1_9.
[3] R. Verduci, et al., Solar energy in space applications: review and technology perspectives, Adv. Energy Mater. 12 (29) (Aug. 2022) 2200125, https://doi.org/10.1002/AENM.202200125.
[4] A. Baiju, M. Yarema, Status and challenges of multi-junction solar cell technology, Front. Energy Res. 10 (Sep. 2022) 971918, https://doi.org/10.3389/FENRG.2022.971918/BIBTEX.
[5] Y. Zhao, et al., Proton radiation hardness and its loss mechanism of Cu2ZnSn(S,Se)4 thin film solar cells, Appl. Phys. Lett. 123 (23) (Dec. 2023), https://doi.org/10.1063/5.0167356/2925724.
[6] Y. Zhao, et al., The degradation of Cu2ZnSn(S,Se)4 kesterite thin film solar cells induced by proton radiation, Adv. Mater. Interfac. 9 (26) (Sep. 2022) 2201049, https://doi.org/10.1002/ADMI.202201049.
[7] Y. Zhao, et al., Radiation hardness of Cu2ZnSn(S,Se)4 thin film solar cells under 10 MeV proton irradiation, Phys. Lett. 472 (Jun. 2023) 128804, https://doi.org/10.1016/J.PHYSLETA.2023.128804.
[8] G.H. Shin, H.S. Lee, Minimal magnetic dipole moment for the solar cell array using GaInP/GaAs/Ge cells, Journal of Electrical Engineering and Technology 15 (3) (May 2020) 1073–1078, https://doi.org/10.1007/S42835-020-00392-Y.
[9] I. Mathews, P.J. King, F. Stafford, R. Frizzell, Performance of III-V solar cells as indoor light energy harvesters, IEEE J Photovolt 6 (1) (Jan. 2016) 230–235, https://doi.org/10.1109/JPHOTOV.2015.2487825.
[10] M. Stan, et al., Very high efficiency triple junction solar cells grown by MOVPE, J. Cryst. Growth 310 (23) (Nov. 2008) 5204–5208, https://doi.org/10.1016/J.JCRYSGRO.2008.07.024.
[11] M. Yamaguchi, F. Dimroth, J.F. Geisz, N.J. Ekins-Daukes, Multi-junction solar cells paving the way for super high-efficiency, J. Appl. Phys. 129 (24) (Jun. 2021), https://doi.org/10.1063/5.0048653.
[12] Photovoltaics in satellites - IEEE spectrum [Online]. Available: https://spectrum.ieee.org/photovoltaics-in-satellites. (Accessed 28 August 2023).
[13] S. Valdueza-Felip, et al., Influence of the AlN interlayer thickness on the photovoltaic properties of in-rich AlInN on Si heterojunctions deposited by RF sputtering, AIP Adv. 8 (11) (Nov. 2018), https://doi.org/10.1063/1.5041924.
[14] R. Blasco, et al., Influence of the AlInN thickness on the photovoltaic characteristics of AlInN on Si solar cells deposited by RF sputtering, Physica Status Solidi (A) Applications and Materials Science 216 (1) (Jan. 2019), https://doi.org/10.1002/PSSA.201800494.
[15] R. Blasco, S. Valdueza-Felip, D. Montero, M. Sun, J. Olea, F.B. Naranjo, Low-to-Mid Al content (x = 0–0.56) AlxIn1−xN layers deposited on Si(100) by radio-frequency sputtering, Phys. Status Solidi B 257 (4) (Apr. 2020), https://doi.org/10.1002/PSSB.201900575.
[16] C. Messmer, M. Bivour, J. Schön, M. Hermle, Requirements for efficient hole extraction in transition metal oxide-based silicon heterojunction solar cells, J. Appl. Phys. 124 (8) (Aug. 2018) 85702, https://doi.org/10.1063/1.5045250/157042.
[17] F. José, P. Zenteno, I. Torres, and R. García-hernansanz, “High Pressure Sputtering of Mo Targets in Mixed Ar/O 2/H 2 Atmospheres for Hole Selective Contacts in Photovoltaic Cells,” pp. 7–10, doi: 10.1109/CDE58627.2023.10339461.
[18] E.S. Andres, et al., High Pressure Sputtering of materials for selective contacts in emerging photovoltaic cells. Proceedings of the 2021 13th Spanish Conference on Electron Devices, CDE 2021, Jun. 2021, pp. 12–14, https://doi.org/10.1109/CDE52135.2021.9455754.
[19] C. Battaglia, et al., Hole selective MoOx contact for silicon solar cells, in: Nano Lett, vol. 14, Feb. 2014, pp. 967–971, https://doi.org/10.1021/NL404389U/SUPPL_FILE/NL404389U_SI_001.PDF, 2.
[20] J. Li, et al., Bilayer MoOX/CrOXPassivating contact targeting highly stable silicon heterojunction solar cells, ACS Appl. Mater. Interfaces 12 (32) (Aug. 2020) 36778–36786, https://doi.org/10.1021/ACSAMI.0C09877.
[21] D. Cheyns, B. Kam, K. Vasseur, P. Heremans, B.P. Rand, Structure induced conductivity enhancement in metal-doped molybdenum oxide thin films, J. Appl. Phys. 113 (4) (Jan. 2013) 43109, https://doi.org/10.1063/1.4789352/818930.
[22] O. Almora, L.G. Gerling, C. Voz, R. Alcubilla, J. Puigdollers, G. Garcia-Belmonte, Superior performance of V2O5 as hole selective contact over other transition metal oxides in silicon heterojunction solar cells, Sol. Energy Mater. Sol. Cell. 168 (Aug. 2017) 221–226, https://doi.org/10.1016/J.SOLMAT.2017.04.042.
[23] Y.C. Jung, Y.J. Yu, Y.K. Kim, J.H. Lee, J.H. Seo, J.Y. Choi, Asymmetric TMO–metal–TMO structure for enhanced efficiency and long-term stability of Si-based heterojunction solar cells, Materials 16 (16) (Aug. 2023) 5550, https://doi.org/10.3390/MA16165550/S1.
[24] A.G. Kuba, et al., The role of oxygen exposure on the performance of all-vapor-processed perovskite solar cells with CuPC hole transport layers, IEEE J Photovolt 14 (5) (Aug. 2024) 758–764, https://doi.org/10.1109/JPHOTOV.2024.3414125.

[25] A. Kuba, et al., The role of oxygen exposure on the performance of all-vapor-processed perovskite solar cells with CuPC hole transport layers. Conference Record of the IEEE Photovoltaic Specialists Conference, Jun. 2021, pp. 1451–1454, https://doi.org/10.1109/PVSC43889.2021.9518616.
[26] A.R. Kirmani, et al., Metal oxide barrier layers for terrestrial and space perovskite photovoltaics, Nat. Energy 8 (2) (2023) 191–202, https://doi.org/10.1038/s41560-022-01189-1.
[27] S.S. Jang, J. Choi, Energy balance analysis of small satellite in low earth orbit (LEO). PECon 2008 - 2008 IEEE 2nd International Power and Energy Conference, 2008, pp. 967–971, https://doi.org/10.1109/PECON.2008.4762613.
[28] Z. Gu, et al., Tunable work function of molybdenum oxynitride for electron-selective contact in crystalline silicon solar cells, Appl. Phys. Lett. 120 (12) (Mar. 2022) 54, https://doi.org/10.1063/5.0086801/2833325.
[29] F.J.P. Zenteno, et al., Fabrication of TiO_x, by high pressure sputtering for selective contact in photovoltaic cells. 2023 14th Spanish Conference on Electron Devices (CDE), Jun. 2023, pp. 1–4, https://doi.org/10.1109/CDE58627.2023.10339432.
[30] R. Garcia-Hernansanz, et al., Deposition of intrinsic a-Si:H by ECR-CVD to passivate the crystalline silicon heterointerface in HIT solar cells, IEEE J Photovolt 6 (5) (Sep. 2016) 1059–1064, https://doi.org/10.1109/JPHOTOV.2016.2581487.
[31] A.B. Morales-Vilches, et al., Study of the surface recombination velocity for ultraviolet and visible laser-fired contacts applied to silicon heterojunction solar cells, IEEE J Photovolt 5 (4) (Jul. 2015) 1006–1013, https://doi.org/10.1109/JPHOTOV.2015.2417757.
[32] L.G. Gerling, S. Mahato, C. Voz, R. Alcubilla, J. Puigdollers, Characterization of transition metal oxide/silicon heterojunctions for solar cell applications, Appl. Sci. 5 (2015) 695–705, https://doi.org/10.3390/APP5040695, 5, no. 4, pp. 695–705, Oct. 2015.
[33] L.G. Gerling, et al., Transition metal oxides as hole-selective contacts in silicon heterojunctions solar cells, Sol. Energy Mater. Sol. Cell. 145 (Feb. 2016) 109–115, https://doi.org/10.1016/J.SOLMAT.2015.08.028.
[34] G. Lindstroem and A. Vasilescu, "Displacement Damage in Silicon," on-line compilation. Accessed: August. 28, 2023. [Online]. Available: https://rd50.web.cern.ch/NIEL/.
[35] J.R. Srour, J.W. Palko, Displacement damage effects in irradiated semiconductor devices, IEEE Trans. Nucl. Sci. 60 (3) (2013) 1740–1766, https://doi.org/10.1109/TNS.2013.2261316.
[36] J. Perez, Why space radiation matters | NASA [Online]. Available: https://www.nasa.gov/analogs/nsrl/why-space-radiation-matters. (Accessed 28 August 2023).
[37] G.R. Hopkinson, C.J. Dale, P.W. Marshall, Proton effects in charge-coupled devices, IEEE Trans. Nucl. Sci. 43 (2 PART 1) (1996) 614–627, https://doi.org/10.1109/23.490905.
[38] K.I. Kurobe, H. Matsunami, New two-diode model for detailed analysis of multicrystalline silicon solar cells, Jpn. J. Appl. Phys., Part 1: Regular Papers and Short Notes and Review Papers 44 (12) (Dec. 2005) 8314–8321, https://doi.org/10.1143/JJAP.44.8314/XML.
[39] M.H. El-Ahmar, A.H.M. El-Sayed, A.M. Hemeida, Mathematical modeling of Photovoltaic module and evalute the effect of varoius paramenters on its performance. International Middle East Power Systems Conference, Jan. 2016, pp. 741–746, https://doi.org/10.1109/MEPCON.2016.7836976.
[40] M. Paulescu, D. Vizman, M. Lascu, R. Negrila, M. Stef, Experimental study of proton irradiation effect on silicon solar cells, AIP Conf. Proc. 1796 (1) (Jan. 2017) 40010, https://doi.org/10.1063/1.4972388/752264.
[41] E.T.P. Benny, J. Majhi, Ultrathin Oxide (SiOx) Grown on HF-Treated Silicon, Feb. 1992, pp. 309–313, https://doi.org/10.1117/12.57010, 1523, doi: 10.1117/12.57010.
[42] R. García-Hernansanz, et al., Transport Mechanisms in Silicon Heterojunction Solar Cells with Molybdenum Oxide as a Hole Transport Layer, 2018, https://doi.org/10.1016/j.solmat.2018.05.019.
[43] L.G. Gerling, C. Voz, R. Alcubilla, J. Puigdollers, Origin of passivation in hole-selective transition metal oxides for crystalline silicon heterojunction solar cells, J. Mater. Res. 32 (2) (Jan. 2017) 260–268, https://doi.org/10.1557/JMR.2016.453/METRICS.
[44] M. Bail, M. Schulz, R. Brendel, Space-charge region-dominated steady-state photoconductance in low-lifetime Si wafers, Appl. Phys. Lett. 82 (5) (Feb. 2003) 757–759, https://doi.org/10.1063/1.1541115.
[45] M. Yamaguchi, K. Ando, A. Yamamoto, C. Uemura, Injection-enhanced annealing of InP solar-cell radiation damage, J. Appl. Phys. 58 (1) (Jul. 1985) 568–574, https://doi.org/10.1063/1.335664.
[46] C.T. Sah, J.Y.C. Sun, J.J. Tzou, S.C.S. Pan, Deactivation of group III acceptors in silicon during keV electron irradiation, Appl. Phys. Lett. 43 (10) (Nov. 1983) 962–964, https://doi.org/10.1063/1.94167.
[47] S.B. Sapkota, M. Fischer, B. Zimmermann, U. Würfel, Analysis of the degradation mechanism of ITO-free organic solar cells under UV radiation, Sol. Energy Mater. Sol. Cell. 121 (Feb. 2014) 43–48, https://doi.org/10.1016/J.SOLMAT.2013.10.021.
[48] A. Alyamani, N. Mustapha, Effects of high dose gamma irradiation on ITO thin film properties, Thin Solid Films 611 (Jul. 2016) 27–32, https://doi.org/10.1016/J.TSF.2016.05.022.
[49] N. Keskitalo, A. Hallén, Resistivity profile measurements of proton-irradiated n-type silicon, Solid State Electron. 37 (1) (Jan. 1994) 55–60, https://doi.org/10.1016/0038-1101(94)90104-X.
[50] R. Blundell, D.V. Morgan, M.J. Howes, Radiation-induced degradation of ohmic contacts, Electron. Lett. 13 (16) (Aug. 1977) 483–484, https://doi.org/10.1049/EL:19770349.
[51] S.J. Brewer, et al., Effect of top electrode material on radiation-induced degradation of ferroelectric thin film structures. J Appl Phys vol. 120, PDF, Jul. 2016 24101, https://doi.org/10.1063/1.4955424/15182846/024101_1_ACCEPTED_MANUSCRIPT, 2.
[52] S.T. Pantelides, The role of extended defects in device degradation, Phys. Status Solidi 210 (1) (Jan. 2013) 175–180, https://doi.org/10.1002/PSSA.201200567.
[53] G. Lulli, E. Albertazzi, M. Bianconi, M. Ferri, Ion-channeling analysis of as relocation in heavily doped Si:As irradiated with high-energy ions, J. Appl. Phys. 94 (9) (Nov. 2003) 6215–6217, https://doi.org/10.1063/1.1616632.
[54] M. Wang, et al., Thermal stability of Te-hyperdoped Si: atomic-scale correlation of the structural, electrical, and optical properties, Phys. Rev. Mater. 3 (4) (Apr. 2019) 044606, https://doi.org/10.1103/PHYSREVMATERIALS.3.044606/FIGURES/6/MEDIUM.
[55] P.M. Voyles, et al., Evidence for a new class of defects in highly n-doped Si: donor-pair-vacancy-interstitial complexes, Phys. Rev. Lett. 91 (12) (2003), https://doi.org/10.1103/PHYSREVLETT.91.125505.
[56] H. Zhu, et al., Evolution of secondary defects in arsenic implanted Si, Jpn. J. Appl. Phys. 55 (4) (Apr. 2016), https://doi.org/10.7567/JJAP.55.045504.
[57] J. Dabrowski, R.A. Casali, H.-J. Müssig, R. Baierle, M.J. Caldas, V. Zavodinsky, Mechanism of dopant segregation to SiO2/Si(001) interfaces, J. Vac. Sci. Technol. B: Microelectronics and Nanometer Structures Processing, Measurement, and Phenomena 18 (4) (Jul. 2000) 2160–2164, https://doi.org/10.1116/1.1306310.
[58] T.F. Schulze, L. Korte, E. Conrad, M. Schmidt, B. Rech, Electrical transport mechanisms in a-Si:H/c-Si heterojunction solar cells, J. Appl. Phys. 107 (2) (2010), https://doi.org/10.1063/1.3267316.
[59] R. Garcia-Hernansanz, et al., Inversion charge study in TMO hole-selective contact-based solar cells, IEEE J Photovolt 13 (5) (Sep. 2023) 656–662, https://doi.org/10.1109/JPHOTOV.2023.3295494.
[60] S. Suckow, T.M. Pletzer, H. Kurz, Fast and reliable calculation of the two-diode model without simplifications, Prog. Photovoltaics Res. Appl. 22 (4) (2014) 494–501, https://doi.org/10.1002/PIP.2301.
[61] S. Rißland, O. Breitenstein, Considering the distributed series resistance in a two-diode model, Energy Proc. 38 (2013) 167–175, https://doi.org/10.1016/J.EGYPRO.2013.07.264.
[62] H. Mimura, Y. Hatanaka, Carrier transport mechanisms of p-type amorphous–n-type crystalline silicon heterojunctions, J. Appl. Phys. 71 (5) (Mar. 1992) 2315–2320, https://doi.org/10.1063/1.351104.
[63] A.N. Nazarov, Y.N. Vovk, V.S. Lysenko, V.I. Turchanikov, V.A. Scryshevskii, S. Ashok, Carrier transport in amorphous SiC/crystalline silicon heterojunctions, J. Appl. Phys. 89 (8) (Apr. 2001) 4422–4428, https://doi.org/10.1063/1.1355698.
[64] B. Jagannathan, W.A. Anderson, Interface effects on the carrier transport and photovoltaic properties of hydrogenated amorphous silicon/crystalline silicon solar cells, Sol. Energy Mater. Sol. Cell. 44 (2) (Nov. 1996) 165–176, https://doi.org/10.1016/0927-0248(96)00042-6.
[65] M. Taguchi, E. Maruyama, M. Tanaka, Temperature dependence of amorphous/crystalline silicon heterojunction solar cells, Jpn. J. Appl. Phys. 47 (2 PART 1) (Feb. 2008) 814–818, https://doi.org/10.1143/JJAP.47.814/XML.
[66] Y.J. Song, M.R. Park, E. Guliants, W.A. Anderson, Influence of defects and band offsets on carrier transport mechanisms in amorphous silicon/crystalline silicon heterojunction solar cells, Sol. Energy Mater. Sol. Cell. 64 (3) (Oct. 2000) 225–240, https://doi.org/10.1016/S0927-0248(00)00222-1.
[67] J. Yu, et al., Heterojunction solar cells with asymmetrically carrier-selective contact structure of molybdenum-oxide/silicon/magnesium-oxide, Sol. Energy 159 (Jan. 2018) 704–709, https://doi.org/10.1016/J.SOLENER.2017.11.047.
[68] M. Bivour, J. Temmler, H. Steinkemper, M. Hermle, Molybdenum and tungsten oxide: high work function wide band gap contact materials for hole selective contacts of silicon solar cells, Sol. Energy Mater. Sol. Cell. 142 (Nov. 2015) 34–41, https://doi.org/10.1016/J.SOLMAT.2015.05.031.
[69] M. Moll, Displacement damage in silicon detectors for high energy physics, IEEE Trans. Nucl. Sci. 65 (8) (Aug. 2018) 1561–1582, https://doi.org/10.1109/TNS.2018.2819506.
[70] H. Matsuura, T. Okuno, H. Okushi, K. Tanaka, Electrical properties of n-amorphous/p-crystalline silicon heterojunctions, J. Appl. Phys. 55 (4) (Feb. 1984) 1012–1019, https://doi.org/10.1063/1.333193.
[71] J.R. Srour, C.J. Marshall, P.W. Marshall, Review of displacement damage effects in silicon devices, IEEE Trans. Nucl. Sci. 50 (3) (Jun. 2003) 653–670, https://doi.org/10.1109/TNS.2003.813197. III.
[72] S.M. Sze, K.K. Ng, Physics of semiconductor devices. Physics of Semiconductor Devices, Oct. 2006, https://doi.org/10.1002/0470068329.
[73] A. Hedler, S.L. Klaumünzer, W. Wesch, Amorphous silicon exhibits a glass transition, Nat. Mater. 3 (11) (2004) 804–809, https://doi.org/10.1038/nmat1241, 3, no. 11, Oct. 2004.
[74] B.G. Svensson, C. Jagadish, J.S. Williams, Generation of point defects in crystalline silicon by MeV heavy ions: dose rate and temperature dependence, Phys. Rev. Lett. 71 (12) (Sep. 1993) 1860, https://doi.org/10.1103/PhysRevLett.71.1860.
[75] B. Yang, Y. Chen, Y. Cui, D. Liu, B. Xu, J. Hou, Over 100-nm-Thick MoOx films with superior hole collection and transport properties for organic solar cells, Adv. Energy Mater. 8 (25) (Sep. 2018) 1800698, https://doi.org/10.1002/AENM.201800698.
[76] O. Concepción, O. de Melo, The versatile family of molybdenum oxides: synthesis, properties, and recent applications You may also like Morphology Controlled Fabrication of Nanostructured Molybdenum Oxides by Different Mineralizers via Hydrothermal Synthesis Method Eren nel and Billur Deniz Karahan-Facile preparation of MoO 3 @Mo 2 CT x the versatile family of molybdenum oxides: synthesis, properties, and recent applications, J. Phys.: Condensed Matter J. Phys.: Condens. Matter 35 (2023) 26, https://doi.org/10.1088/1361-648X/acb24a.